

博士論文

論文題目

Towards specific inhibition of SIRT2 deacetylase by a
macrocyclic peptide inducing dynamic structural change

〔環状ペプチドにより惹起されるサーチュイン2の
構造変化、及び特異的阻害剤に向けて〕

Kenichiro Yamagata

山形 研一郎

Table of contents

Abstract	3
Introduction	4
Experimental Procedures	9
Chemical synthesis of macrocyclic peptides	9
Protein preparation	11
Crystallography	15
Surface plasmon resonance analysis	18
Results and Discussion	19
Crystal structure of human SIRT2 in complex with S2iL5	19
S2iL5 recognition by SIRT2	22
Structural change upon S2iL5 binding	35
Mutational analysis	43
Structural plasticity of macrocyclic peptide inhibitors	46
References	48
Acknowledgments	55

Abstract

SIRT2 deacetylates specific acetyllysine residues in diverse proteins, and is implicated in a variety of cellular processes. SIRT2 inhibition thus has potentials to treat human diseases, such as cancers and neurodegenerative disorders. I have recently developed a series of ϵ -trifluoroacetyllysine-containing macrocyclic peptides, which inhibit the SIRT2 activity more potently than most other known inhibitors. Here I report the crystal structure of human SIRT2 in complex with a macrocyclic peptide inhibitor, S2iL5, at 2.5-Å resolution. The structure revealed that S2iL5 binds to the active site of SIRT2 through extensive interactions. A structural comparison of the SIRT2–S2iL5 complex with SIRT2 in the free form and in complex with ADP-ribose revealed that S2iL5 induces an open-to-closed domain movement and an unexpected helix-to-coil transition in a SIRT2-specific region. My findings unveiled the potential of macrocyclic peptides to bind target proteins by inducing dynamic structural changes.

Introduction

Sirtuins are a family of evolutionarily conserved, nicotinamide adenine dinucleotide (NAD⁺)-dependent deacetylases¹. NAD⁺ functions as a co-substrate during the deacetylation reaction, such that the carbonyl oxygen of the ϵ -acetylamide group first attacks the C1' of the N-ribose in NAD⁺ to form an *O*-alkylamidate intermediate upon the release of a nicotinamide group, and following several reaction steps give the free ϵ -amino-K residue and 2'-*O*-acetyl-ADP-ribose (Figure 1A). The seven mammalian sirtuins, SIRT1–SIRT7, have distinct substrate specificities and subcellular localizations, and are implicated in a variety of biological processes, such as gene silencing, cell-cycle regulation, metabolism, apoptosis, longevity and cancer (Table 1)^{2,3}. SIRT2 is primarily localized in the cytoplasm and nucleus, and it deacetylates specific acetyllysine residues in diverse proteins. For instance, the SIRT2-catalyzed deacetylation of α -tubulin^{4,5} and histone H4^{4,6} functions in the regulation of cell-cycle progression, and its deacetylation of receptor-interacting protein 1 (RIP1) is responsible for the modulation of RIP1–RIP3 complex formation, and thus regulates programmed necrosis⁷. In addition, the siRNA-mediated down-regulation of SIRT2 induces apoptosis in HeLa cells, caused by p53 accumulation⁸. Moreover, SIRT2 is associated with the aggregation of neural proteins such as α -synuclein⁹ and huntingtin¹⁰, and thus

SIRT2 inhibition prevents neurodegeneration in Parkinson's disease⁹ and Huntington's disease¹⁰ models. Collectively, the specific inhibition of SIRT2 has tremendous potentials to treat various human diseases.

High-throughput and *in silico* screening campaigns have identified more than a dozen distinct inhibitors against a family of sirtuins¹¹⁻¹³, including SRT1720¹⁴, Ex-527¹⁵, Suramin¹⁶, thieno[3,2-*d*]pyrimidine-6-carboxamide-based inhibitors¹¹⁻¹³, and indole-based inhibitors¹¹⁻¹³. Crystallographic studies revealed that SRT1720¹⁴ and Ex-527¹⁵ occupy the peptide substrate- and NAD⁺-binding sites of sirtuins, respectively, and that Suramin¹⁶ and the thieno[3,2-*d*]pyrimidine-6-carboxamides¹¹⁻¹³ occupy both the peptide substrate- and NAD⁺-binding sites. In addition, several mechanism-based peptidic inhibitors have also been developed¹⁷. These inhibitors have an inert or poorly reactive moiety, such as ϵ -trifluoroacetylamine on lysine (K^{Tfa})¹⁸, which probably occupies the ϵ -acetylamine binding site of sirtuins (Figure 1B). However, most of these inhibitors exhibit modest potency and isoform-selectivity. Recently, I constructed a library of K^{Tfa}-containing macrocyclic peptides and screened for active species that strongly bind SIRT2¹⁹, by means of the RaPID (random nonstandard peptide integrated discovery) system^{20,21}. The discovered macrocyclic peptides are able to bind SIRT2 with dissociation constants (K_{DS}) in the low nanomolar range, and they inhibit the

deacetylase activity with a similar range of IC_{50} values. Macrocyclic peptides usually show increased protease-resistance and potentially better cell permeability than linear peptides, and thus can serve as a preferred scaffold for drug development, as exemplified by the immunosuppressive cyclic peptide cyclosporin A ²². Although the RaPID system is a suitable technology to discover such potent macrocyclic peptides, including the aforementioned anti-SIRT2 inhibitors, it remains unclear how these macrocyclic peptides strongly bind SIRT2 and exhibit their inhibitory activities.

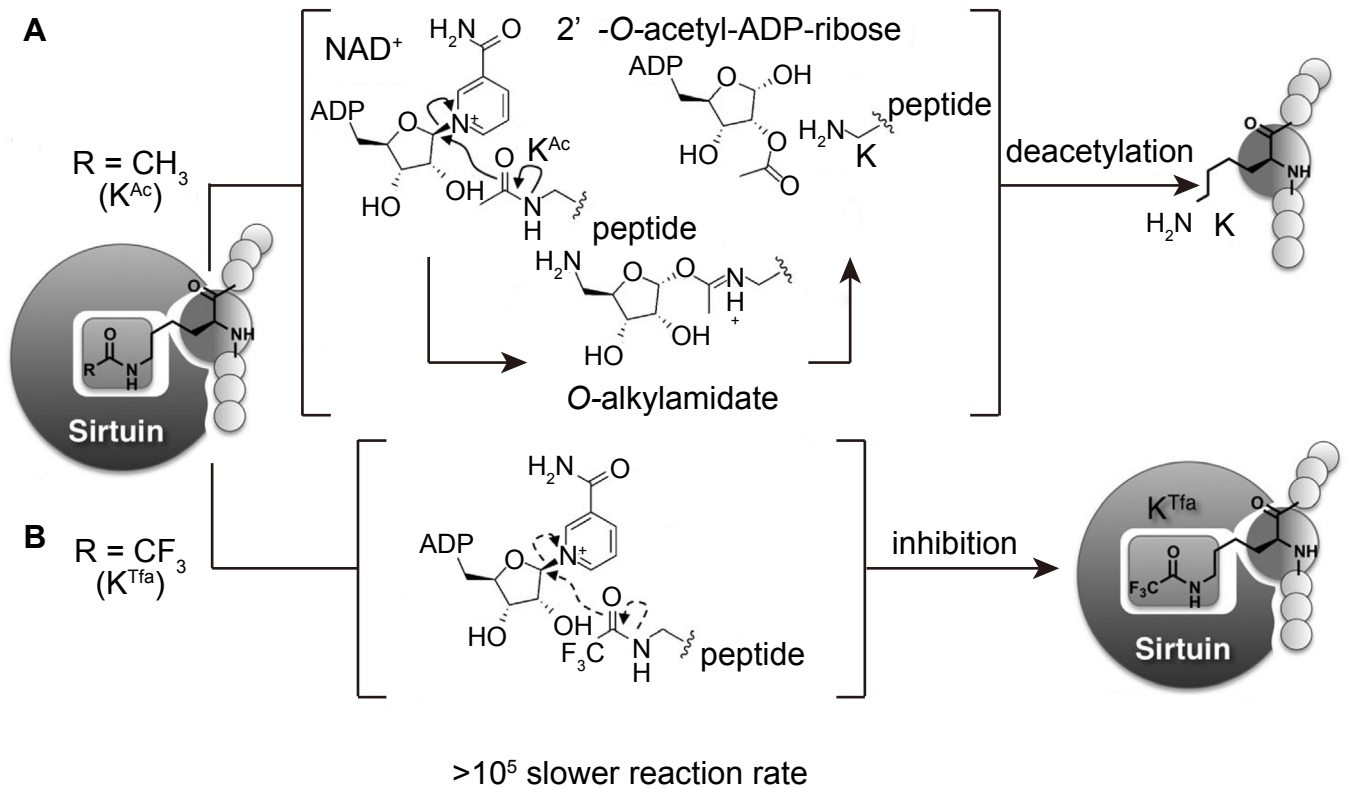


Figure 1 Reaction mechanism of sirtuins

(Quoted from *Morimoto et al. 2012*)

(A) Deacetylation mechanism of Sirtuin with peptides with ϵ -acetylamine on lysine. ϵ -amino-K residue and 2' - O -acetyl-ADP-ribose is produced.

(B) The inhibition mechanism of sirtuin by peptides with ϵ -trifluoroacetylamine on lysine. ϵ -trifluoroacetylamine is supposed to occupy the ϵ -acetylamine binding site, resulting in inhibition of sirtuin reaction.

Table 1. Function of human Sirtuin families

Sirtuin	Localization	Activity	Targets	Key functions
SIRT1	Nucleus and cytosol	Deacetylase	PGC-1 α , FOXOs, NF κ B, p53	Metabolism, Inflammation
SIRT2	Nucleus and Cytoplasm	Deacetylase	H4, α -tubulin, RIP1, p53	Cell cycle, Necrosis, Myelination
SIRT3	Mitochondria	Deacetylase	AceCS2, PGC-1a	Fatty acid oxidation, Antioxidant defences
SIRT4	Mitochondria	ADP-ribosyltransferase	GDH	Insulin secretion, Suppression of fatty acid oxidation
SIRT5	Mitochondria	Deacetylase Demalonylase Desuccinylase	Unknown	Urea cycle
SIRT6	Nucleus	Deacetylase ADP-ribosyltransferase	DNA polymerase β	Genome stability, Metabolism
SIRT7	Nucleolus	Deacetylase	RNA polymerase I	Ribosomal DNA transcription

Experimental Procedures

Chemical synthesis of macrocyclic peptides

The S2iL5 peptide and its mutants were synthesized with amidated C-termini by standard Fmoc-based solid phase peptide synthesis. NovaPEG Rink Amide resin (Novabiochem) was used as the solid support. For the cyclized peptides, after elongation of the peptide chain, the resulting N-terminal α -amino group was chloroacetylated by an incubation with a solution of 0.2 M chloroacetyl *N*-hydroxysuccinimide ester in DMF, with rotation for 40 min at room temperature. For the linear peptides, the N-terminal amino group was acetylated by an incubation with a solution of 0.5 M acetic anhydride and 0.25 M *N,N*-diisopropylethylamine in DMF, for 40 min at room temperature. After washing the resin with DMF (2 ml, 3 times) and DCM (2 ml, 6 times), the peptides were cleaved from the resin and deprotected by an incubation with a solution of trifluoroacetic acid (TFA)/1,2-ethanedithiol/triisopropyl silane/water (92.5 : 2.5 : 2.5 : 2.5), with rotation at room temperature for 3 h. The solutions were concentrated *in vacuo*, and the cleaved peptides were then precipitated with diethyl ether. For cyclization, the resulting peptide pellets were dissolved in 20 ml of water/DMSO (1:1), and triethylamine was added to the solution to bring its pH to

around ten. After an incubation at room temperature for 30 min to promote the cyclization, the peptide solution was acidified by TFA and purified by reverse-phase HPLC, using a gradient of eluent B (0.1% TFA in acetonitrile) in eluent A (0.1% TFA in water). The purified peptides were lyophilized and dissolved in DMSO.

Protein preparation

The gene encoding human SIRT2 (residues 1–370) was amplified by PCR, and cloned between the *Nde*I and *Xho*I sites of the modified pET28a vector (Novagen). The protein was expressed at 20°C in *Escherichia coli* Rosetta 2 (DE3) (Novagen), and purified by Ni-NTA Superflow resin (QIAGEN). The eluted protein was incubated with trypsin (1:100, w/w) for 2.5 h at 4°C, since limited trypsin proteolysis of SIRT2 was found to produce a stable 36 kDa fragment, which was determined to be SIRT2 (residues 43–370) using MALDI-TOF MS (Figure 2). The protein was further purified by chromatography on Resource Q (GE Healthcare) and HiLoad Superdex 200 16/60 (GE Healthcare) columns (Figures 3 and 4). The purified protein was concentrated using an Amicon Ultra 30K filter (GE Healthcare). The expression vectors for the SIRT2 mutants were generated by a PCR-based method, using the expression vector for full-length SIRT2 as a template, and the sequences were verified by DNA sequencing. The mutant proteins were expressed at 20°C in *E. coli* Rosetta 2 (DE3), and purified with Ni-NTA Superflow resin.

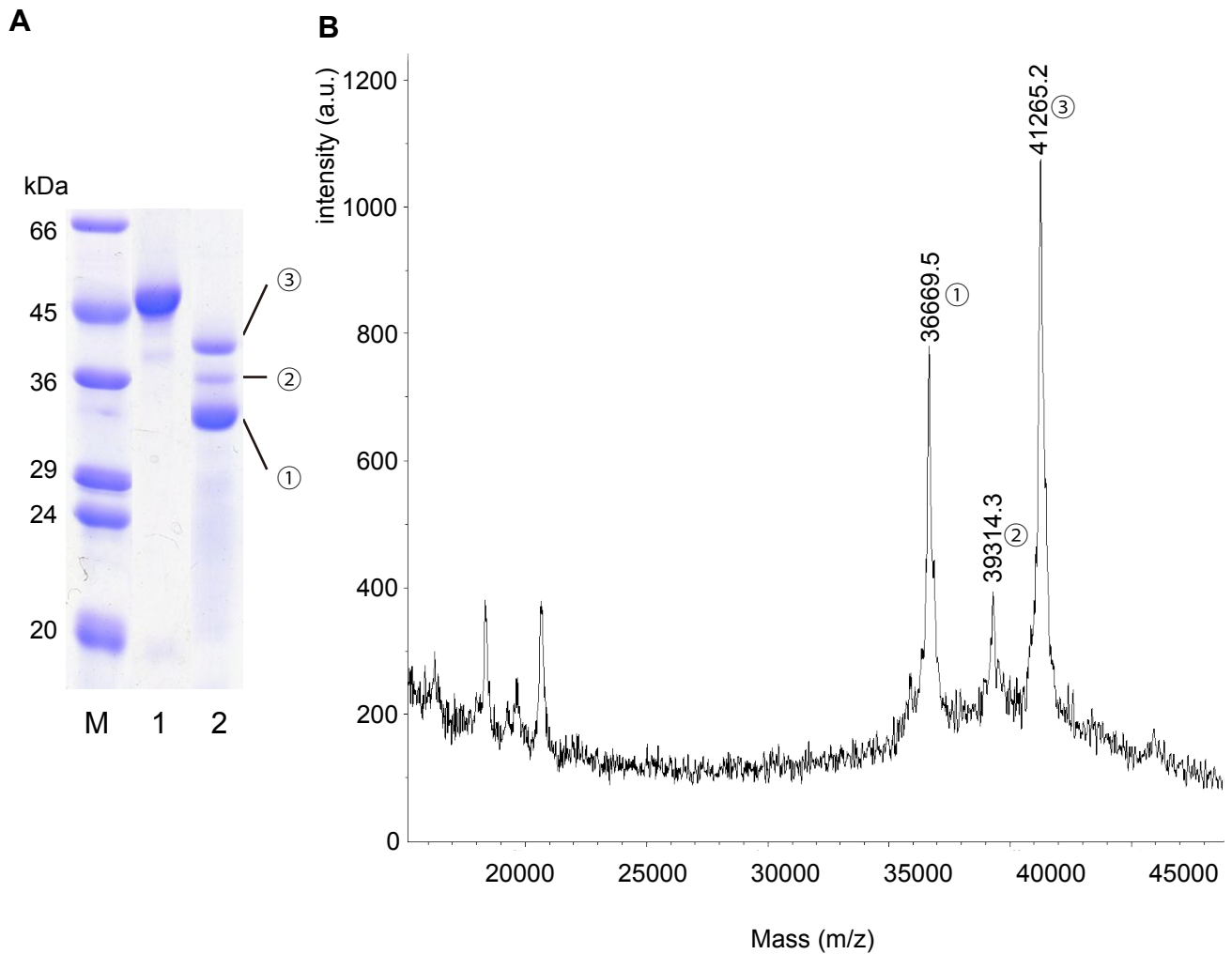


Figure 2 SDS-PAGE and MALDI-TOF MS after trypsin digestion of SIRT2

(A) SDS-PAGE of SIRT2 before and after trypsin digestion. M, marker; 1, expressed SIRT2 with His-Tag; 2, SIRT2 after trypsin digestion. Three major components were found (①-③) and performed MALDI-TOF MS.

(B) Results of MALDI-TOF MS after trypsin digestion. Molecular weight of ①-③ were determined to be 36669.5, 39314.3, 41265.2, respectively. The main component (= ①) is supposed to be SIRT2 of residues 43-370.

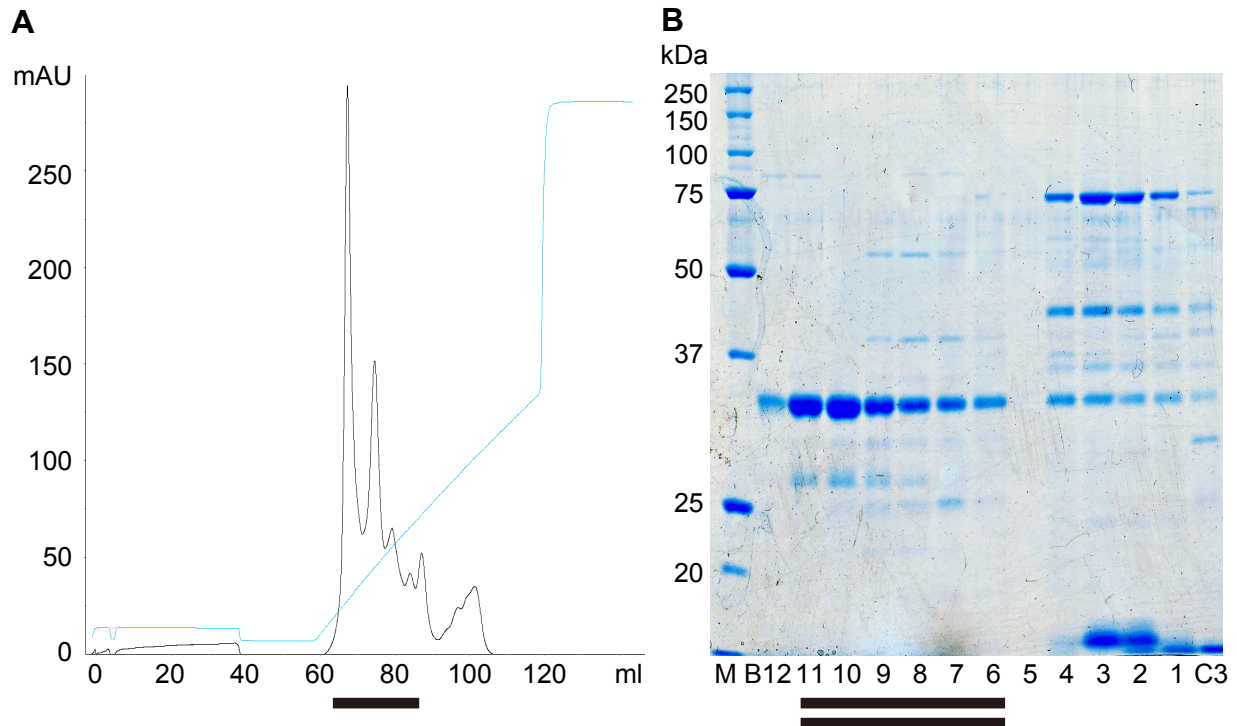


Figure 3 Purification of SIRT2 with Resource Q

(A) Purification of SIRT2 with Resource Q. The output is in black and the gradient of 0.5 M NaCl is in skyblue. Fractions with underline were collected for SDS-PAGE.

(B) SDS-PAGE of SIRT2 after Resource Q. M, marker; B12 to C3 are fractions of Resource Q. B11-B6 (indicated with double underline) were collected for further purification.

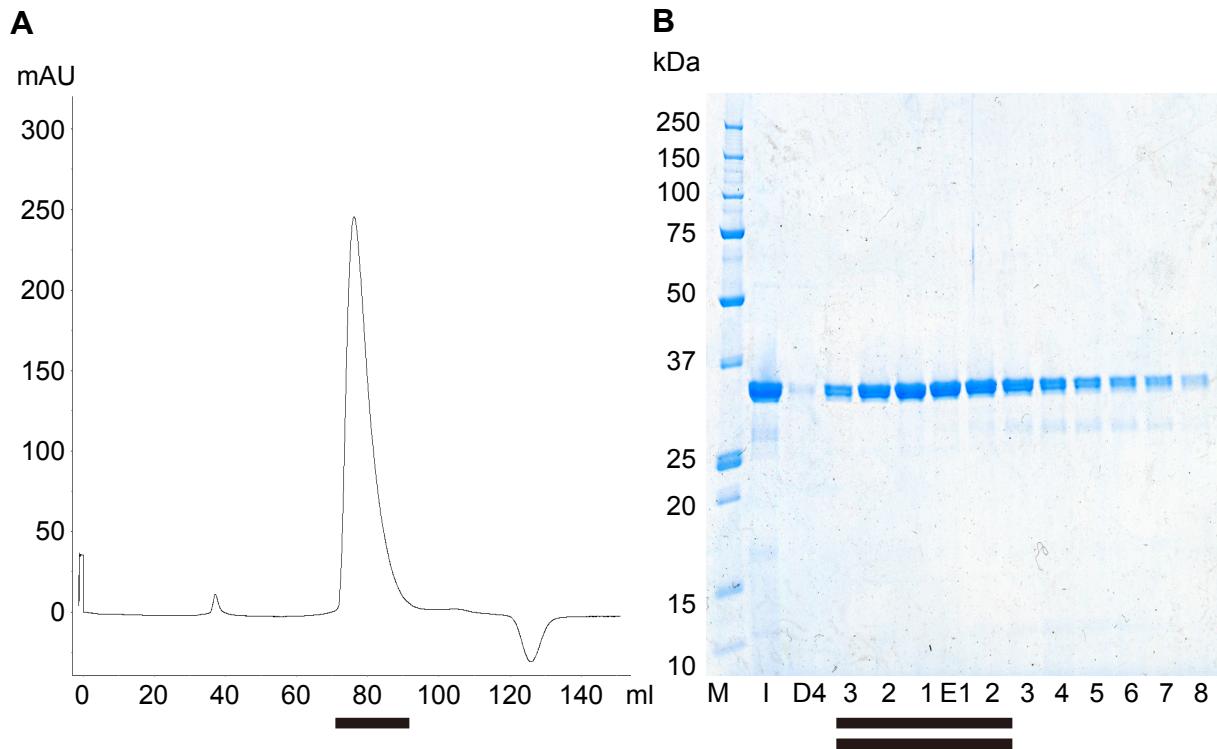


Figure 4 Purification of SIRT2 with SPDX 200

(A) Purification of SIRT2 with SPDX 200. Fractions with underline were collected for SDS-PAGE.

(B) SDS-PAGE of SIRT2 after SPDX 200. M, marker; I, input sample; D4 to E8 are fractions of SPDX 200. D3-E2 (indicated with double underline) were collected for crystallization.

Crystallography

Purified SIRT2 (residues 43–370) was crystallized at 4°C by the sitting-drop vapor diffusion method. SIRT2 (10 mg ml⁻¹) was mixed with S2iL5 at a 1:2 (SIRT2:S2iL5) molar ratio in 20 mM Tris-HCl, pH 8.0, 150 mM NaCl and 1 mM DTT. Crystals were obtained by mixing 0.5 µl of protein solution and 0.5 µl of reservoir solution (100 mM MES-NaOH, pH 7.0, 100 mM Li₂SO₄, 100 mM NaCl and 8.5% PEG 4,000) (Figure 5). X-ray diffraction data were collected at 100 K on the beamline BL32XU at SPring-8 (Hyogo, Japan) (Figure 6). The crystals were cryoprotected in reservoir solution supplemented with 30% ethylene glycol. X-ray diffraction data were processed using HKL2000 (HKL Research, Inc.). The structure was determined by molecular replacement with MOLREP²³, using the SIRT2 structure in the free form (PDB ID 1J8F) as a search model. The model was built manually using COOT²⁴ and refined using PHENIX²⁵. The final model contains four SIRT2–S2iL5 complexes (residues 55–98 and 104–356 for Mol A, residues 56–100 and 107–356 for Mol B, residues 57–99 and 106–356 for Mol C, and residues 57–98 and 106–356 for Mol D), four zinc ions, and four MES, four ethylene glycol and 507 water molecules. Molecular graphic images were prepared using CueMol (<http://www.cuemol.org>).

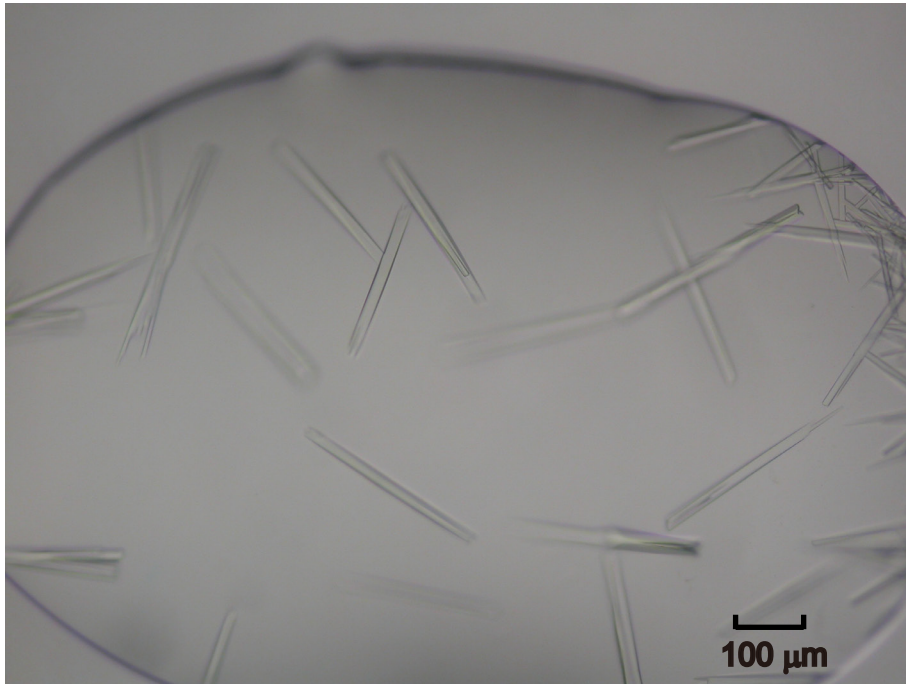


Figure 5 Crystals of SIRT2-S2iL5 complex

Needle crystals of 400 μm were obtained.

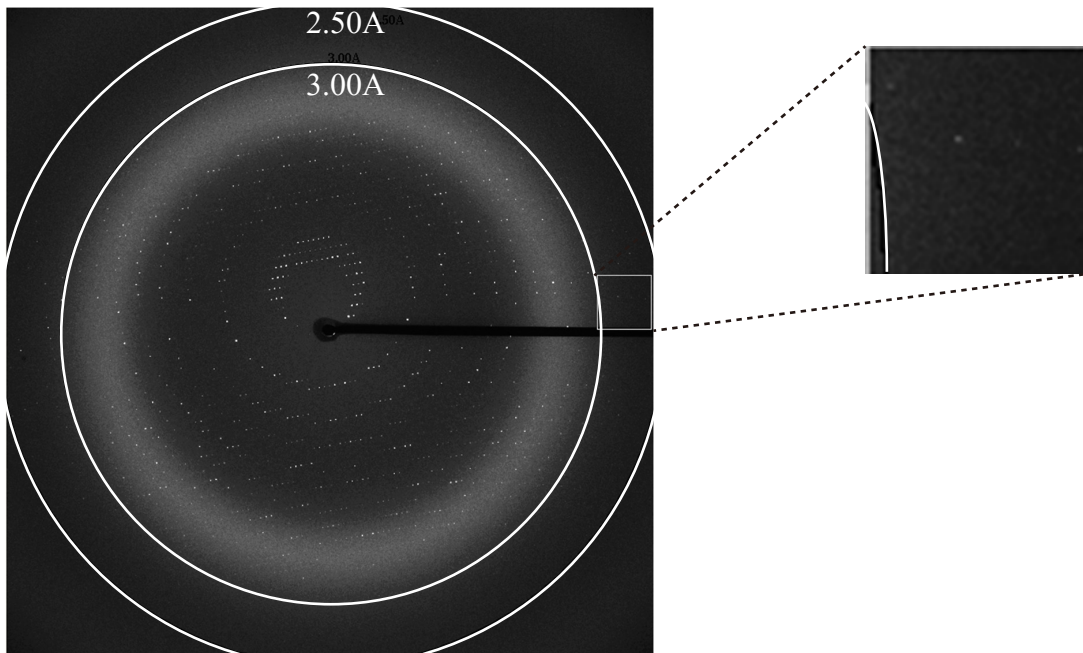


Figure 6 Diffraction pattern of SIRT2-S2iL5 complex

Obtained diffraction pattern obtained at SPring-8 BL32XU. The diffraction around 2.5 Å is enlarged.

Surface plasmon resonance analysis

SPR measurements were performed at 10°C on a Biacore T200 instrument (GE Healthcare) equipped with a Ni-NTA sensor chip. Modified HBS-EP+ (10 mM HEPES-KOH, pH 7.4, 150 mM NaCl, 50 μ M EDTA, 0.05% Tween 20, 0.1% DMSO) was used as the running buffer for all experiments. To collect kinetics data, a series of five different concentrations of each peptide was injected for 1 min at a flow rate of 30 μ l min⁻¹. Dissociation of the peptide was allowed to continue for 1 min between injections and 5 min after the final injection. Buffer blank injections were performed before and after the sample injection for double referencing with a negative control surface without protein immobilization, to monitor the background binding. Binding sensorgrams were fitted with the Biacore evaluation software.

Results and Discussion

Crystal structure of human SIRT2 in complex with S2iL5

To gain structural insights into their inhibitory mechanisms, I performed crystallization screening of human SIRT2 in the presence of several macrocyclic peptides, and successfully determined the crystal structure of SIRT2 in complex with one of the inhibitor peptides, S2iL5, at 2.5-Å resolution (Table 2 and Figure 7). The structure revealed that SIRT2 consists of a large Rossmann-fold domain (residues 55–91, 146–186 and 241–356) and a small zinc-binding domain (residues 92–145 and 187–240) (Figure 7), as in the structure of SIRT2 in the free form²⁶ (Figure 8). The asymmetric unit contains four SIRT2–S2iL5 complexes (Mol A–Mol D), which are essentially identical (r.m.s. deviation values for C α atoms are less than 0.70 Å) (Figure 9). Thus, I will hereafter describe Mol A.

S2iL5 consists of 14-amino acid (aa) residues cyclized via a thioether bond (Figure 10), and exhibits remarkably high affinity and inhibitory activity against SIRT2 ($K_D = 1.0$ nM at 10°C and $IC_{50} = 13$ nM at 37°C) (Figures 11 and 12). The bound S2iL5 is clearly defined in the $F_O - F_C$ omit electron density map (Figure 13; the SIRT2 and S2iL5 residues are denoted by the three-letter and one-letter codes, respectively). S2iL5

adopts a unique cyclic structure, which is stabilized by multiple intramolecular hydrogen bonds. The side chain of R8 is flipped inside the cyclic scaffold, and its guanidine head is nearly in the center. This positioning of the guanidine head is supported by direct hydrogen bonds with the carbonyl groups of Y4 and V6 and water-mediated hydrogen bonds with the carbonyl groups of R9 and N11. This R8 residue adjacent to the K^{Tfa} is highly conserved among the selected macrocyclic peptide inhibitors¹⁹, suggesting that it plays a crucial role in maintaining their tertiary structural integrity. Moreover, hydrogen-bonding interactions are formed between T3 and V6 and between H2 and the carbonyl group around the thioether linkage. This structure allows the presentation of the K^{Tfa7} side chain outside the cyclic scaffold, for binding to SIRT2. I refer to this unique peptide structure as a “power button icon”-like (PBI-like) macrocycle, due to the shape similarity (Figure 10).

Table 2. Data collection and refinement statistics

SIRT2–S2iL5	
Data collection	
Space group	<i>P</i> 2 ₁ 2 ₁ 2 ₁
Cell dimensions	
<i>a</i> , <i>b</i> , <i>c</i> (Å)	91.18, 135.61, 148.83
α , β , γ (°)	90, 90, 90
Resolution (Å)	50.0–2.52 (2.56–2.52)*
<i>R</i> _{sym}	0.148 (0.410)
<i>I</i> / σ <i>I</i>	14.8 (3.4)
Completeness (%)	98.6 (96.6)
Redundancy	5.2 (3.9)
Refinement	
Resolution (Å)	46.6–2.52 (2.56–2.52)
No. reflections	61,346
<i>R</i> _{work} / <i>R</i> _{free}	0.216 / 0.263
No. atoms	
Protein	9,323
Ligand/ion	644
Water	507
<i>B</i> -factors	
Protein	36.1
Ligand/ion	24.5
Water	27.6
R.m.s. deviations	
Bond lengths (Å)	0.003
Bond angles (°)	0.605

*Values in parentheses are for highest-resolution shell.

S2iL5 recognition by SIRT2

S2iL5 binds to the active-site groove between the small and large domains of SIRT2, with the K^{Tfa}7 side chain inserted into the catalytic tunnel formed by His187, Val233 and Phe235 (Figures 14 and 15A). This is the first crystal structure of sirtuin in complex with a K^{Tfa}-containing peptide, and it confirmed that the K^{Tfa} residue occupies the acetyllysine-binding site of sirtuin. The hydrocarbon chain of K^{Tfa}7 is sandwiched by the side chains of His187 and Phe235, with its N ϵ atom hydrogen bonded to the carbonyl group of Val233 (Figures 14 and 15A). The amide and carbonyl groups of K^{Tfa}7 hydrogen bond with the carbonyl group of Glu237 and the amide group of Gly236 in the small domain, respectively. In addition, the amide and carbonyl groups of R8 hydrogen bond with the carbonyl and amide groups of Gln267 in the large domain, respectively. Consequently, SIRT2 and S2iL5 (K^{Tfa}7 and R8) form an intermolecular β sheet-like interaction (Figures 14 and 15A). His187, Val233 and Phe235 are highly conserved among the sirtuin family members (Figure 15B), and the acetyllysine residues of the substrate peptides are recognized in a similar manner in other sirtuin–substrate peptide complex structures²⁷⁻³¹. For instance, in the SIRT3–AceCS-K^{Ac}642 complex structure, the side chain of K^{Ac}642 is sandwiched by the side chains of His248 and Phe294, with its N ϵ atom hydrogen bonded to the carbonyl

group of Val292 (Jin et al., 2009) (Figure 15B). The amide and carbonyl groups of K^{Ac}642 hydrogen bond with the carbonyl group of Glu296 and the amide group of Gly295, respectively, and the amide and carbonyl groups of V643 hydrogen bond with the carbonyl and amide groups of Glu325, respectively.

In addition to these interactions commonly observed in sirtuins, S2iL5 forms a number of hydrophilic and hydrophobic interactions with SIRT2, with a buried surface area of 845 Å² (42% of the total surface area of S2iL5), which is larger than that for the SIRT3–AceCS-K^{Ac} complex (582 Å²) (Figures 14 and 15A). The R9 side chain of S2iL5 forms salt bridges with Glu116 and Glu120, and a cation- π interaction with Phe235. Y4, H5 and T10 of S2iL5 hydrogen bond with Ser271, Leu239 and Gln265, respectively. The side chains of Y4 and H5 in S2iL5 form van der Waals interactions with the side chain of Phe244, which in turn forms an edge-to-face interaction with Phe243. In addition, S2iL5 interacts with a SIRT2-specific insertion loop (residues 289–304) in the large domain (Figures 14 and 15A). Y12 of S2iL5 hydrogen bonds with Asp294, and Y1 and Y12 form van der Waals interactions with the side chain Met299, and Phe296 and Met301, respectively. The insertion loop is unique to SIRT2 (Figure 16), thus partly explaining why S2iL5 binds SIRT2 ($K_D = 1.0$ nM) more potently than SIRT3

($K_D = 1.8$ nM) (Figure 11A). Altogether, the present structure revealed that S2iL5 adopts a PBI-like structure to achieve extensive interactions with SIRT2.

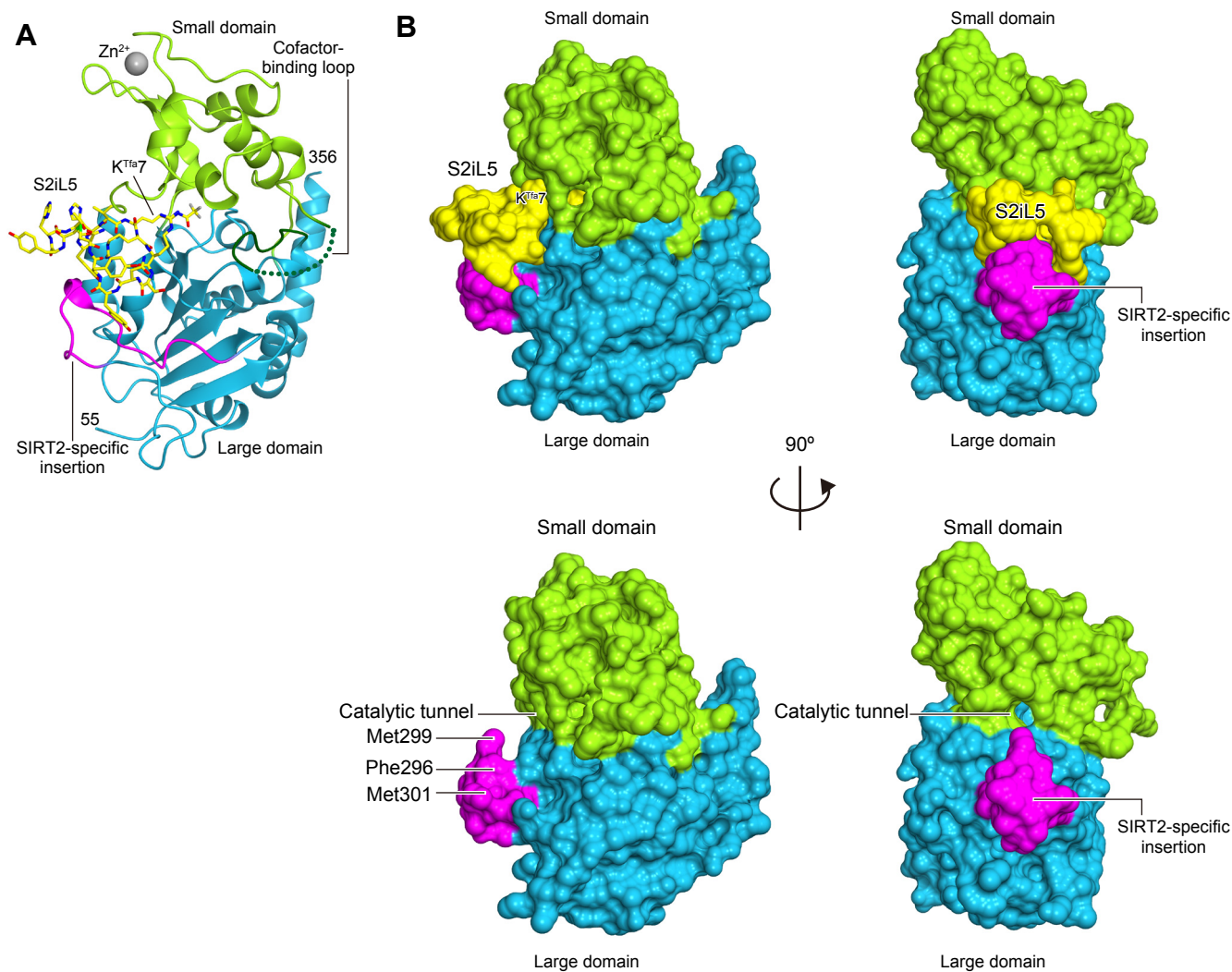


Figure 7 Crystal structure of SIRT2-S2iL5 complex

(A) Overall structures of SIRT2 in complex with S2iL5. The small and large domains are colored yellow-green and cyan, respectively. S2iL5 is shown as a stick model, in which the carbon atoms are yellow, oxygen atoms are red, nitrogen atoms are blue and the fluorine atom is gray. The bound zinc ion is shown as a gray sphere. The cofactor-binding loop (residues 92–104) and the SIRT2-specific insertion (residues 289–304) are colored green and magenta, respectively. The disordered region (residues 99–103) in the S2iL5 complex is indicated by green dots.

(B) Molecular surfaces of SIRT2 in the complex with S2iL5. The molecular surface of SIRT2 alone, in which S2iL5 is omitted from the complex, is also shown.

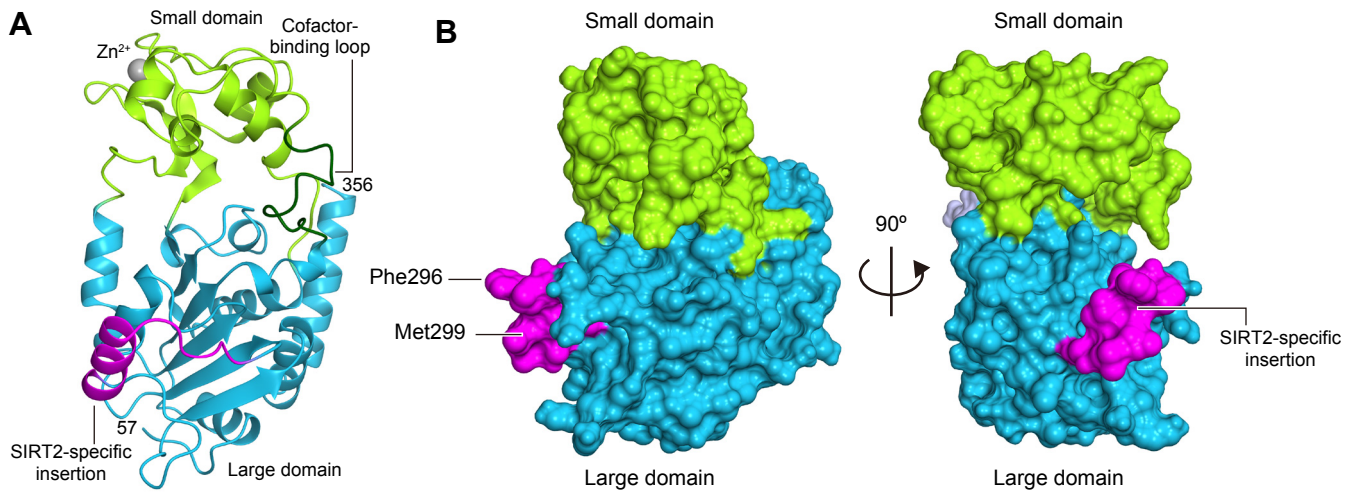


Figure 8 Crystal structure of SIRT2 in free form

(A) Overall structures of SIRT2 in the free form. SIRT2 is colored as in Figure 7.

(B) Molecular surfaces of SIRT2 in the free form.

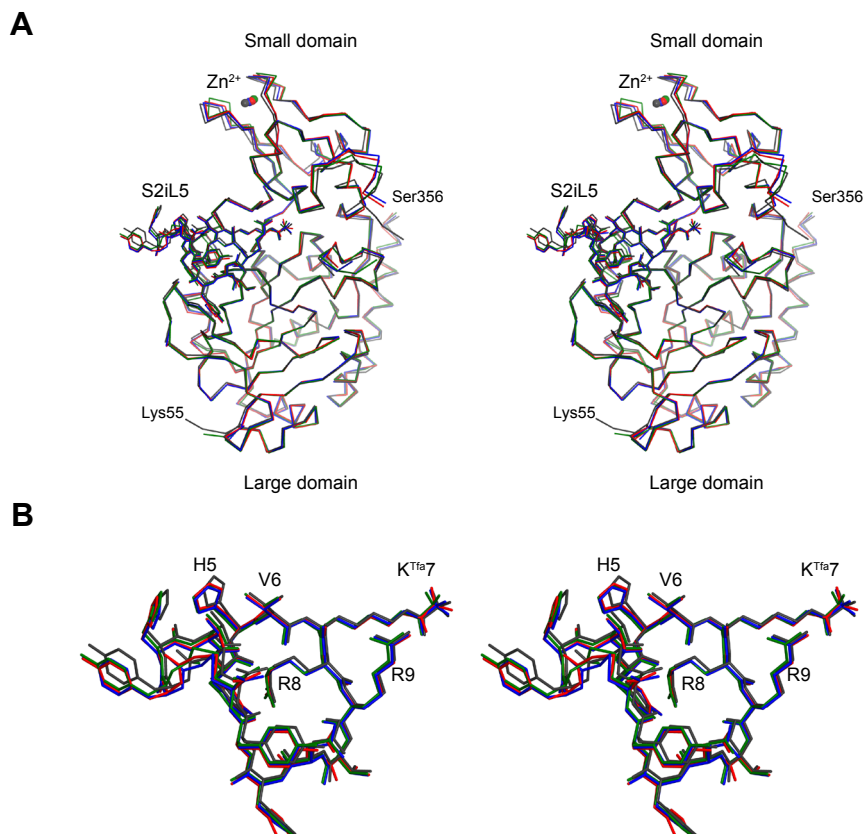


Figure 9 Superimposition of the four SIRT-S2iL5 molecules

(A) Superimposition of the four SIRT2–S2iL5 complexes in the asymmetric unit (stereo view). The bound zinc ions are shown as spheres. Mol A–Mol D are colored gray, green, blue and red, respectively.

(B) Superimposition of S2iL5 in Mol A–Mol D (stereo view).

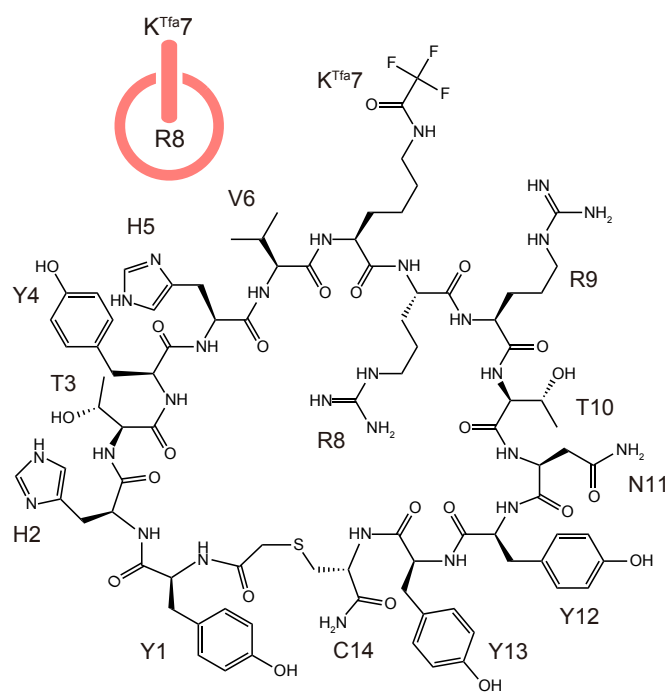


Figure 10 Chemical structure of S2iL5

Chemical structure of S2iL5. The peptide is cyclized via a thioether bond between Y1 and C14.

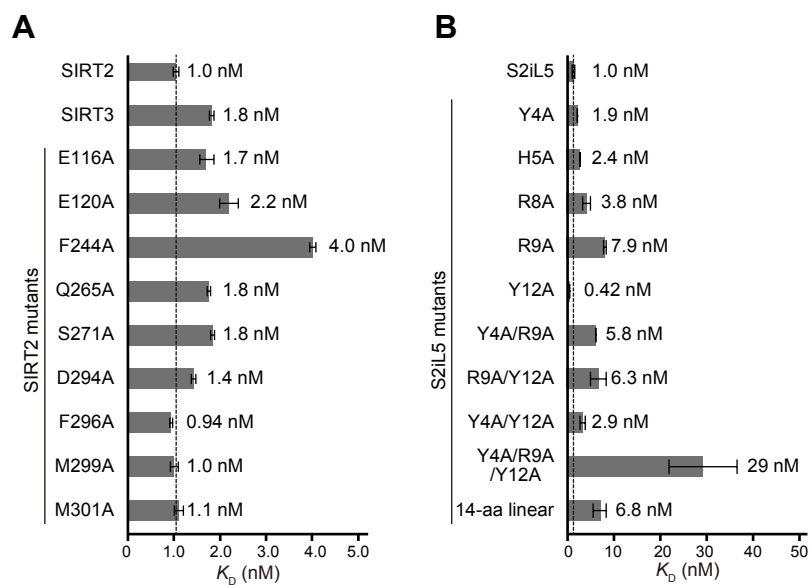


Figure 11 Results of the Surface plasmon resonance analysis

(A) Binding of S2iL5 to SIRT3 and the alanine mutants of SIRT2

(B) Binding of the alanine mutants of S2iL5 to SIRT2.

In (A) and (B), the K_D values were determined by SPR experiments and are shown as means \pm s.d. (n = 3).

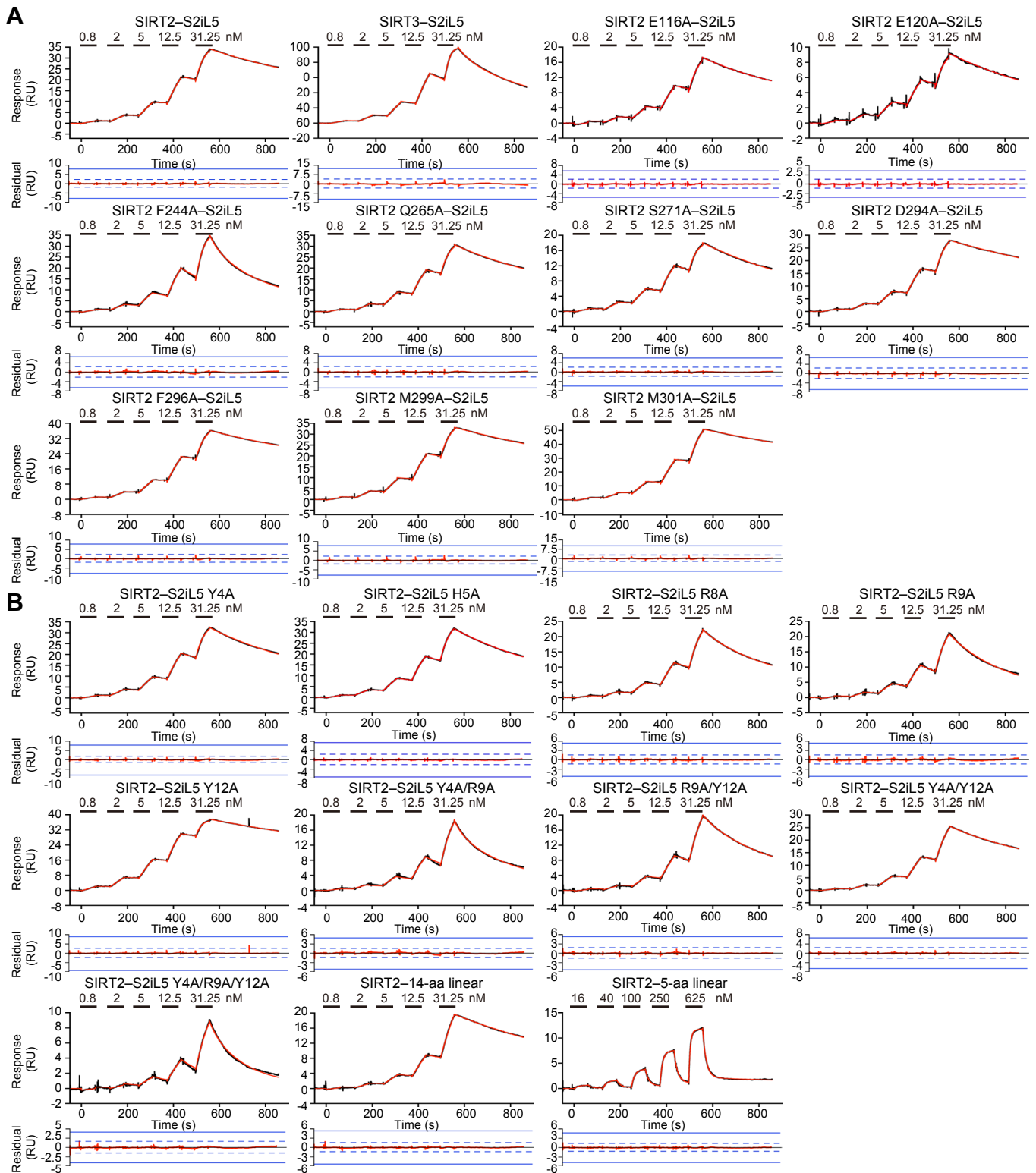


Figure 12 Raw data of the Surface plasmon resonance analysis

(A, B) SPR sensorgrams of interactions between SIRT2 (A) and the S2iL5 (B) mutants. The sensorgrams were obtained using the single-cycle kinetics method, by adding peptides to a SIRT2-immobilized sensor chip. The raw data (black) were superimposed to theoretical fitting curves based on a 1:1 binding model (red). Concentrations of added peptide are shown above the sensorgrams.

In (A) and (B), residual plots of the fitting curves are shown at the bottom of sensorgrams.

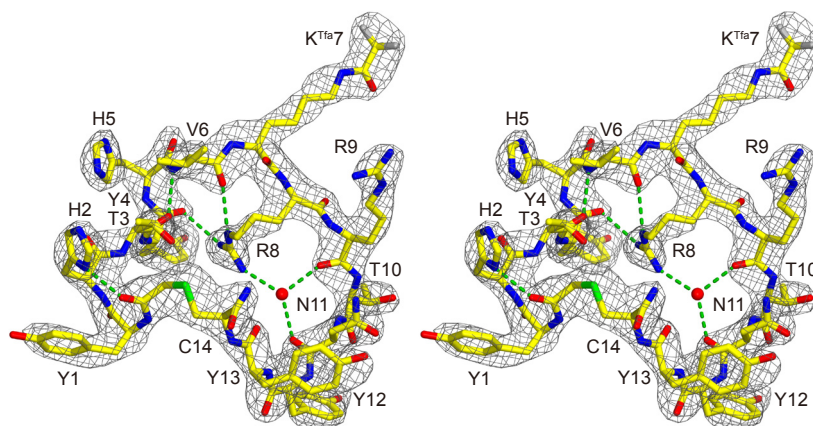


Figure 13 *mFO-DFC* omit electron density map of S2iL5

Structure of S2iL5 (stereo view). The *mFO – DFC* omit electron density map for S2iL5 is shown as a gray mesh (contoured at 4σ). S2iL5 is colored as in Figure 7. A water molecule is shown as a red sphere and hydrogen bonds are shown as green dashed lines.

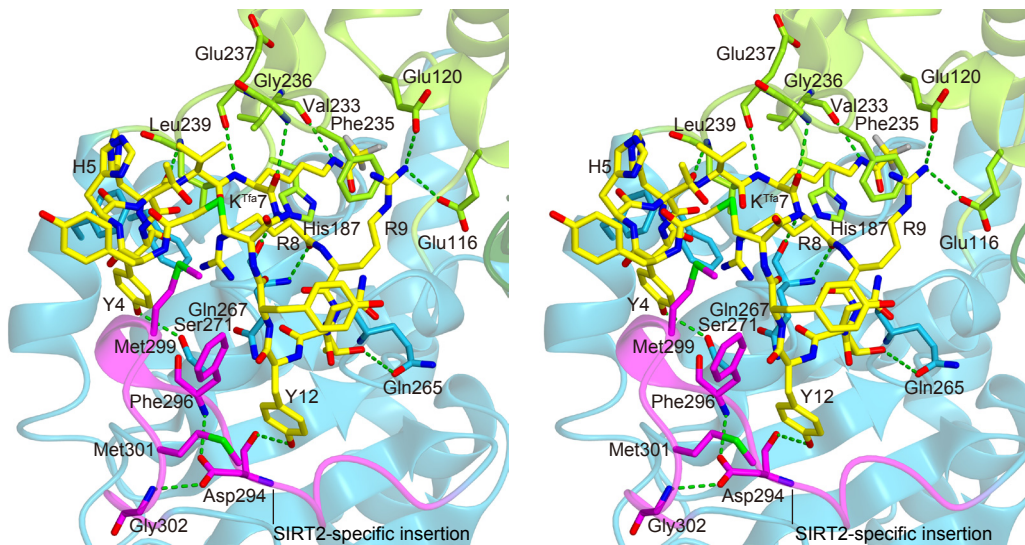


Figure 14 S2iL5 recognition by SIRT2

S2iL5 recognition by SIRT2 (stereo view). Hydrogen bonds are shown as green dashed lines.

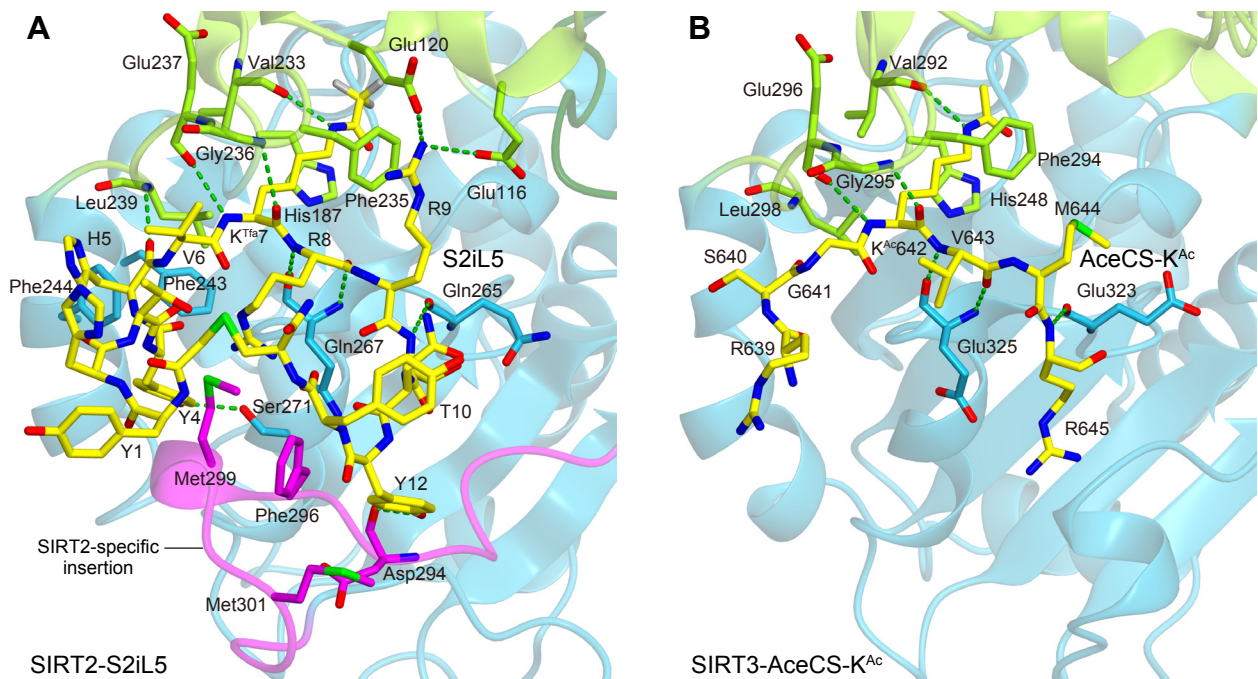


Figure 15 Structural comparison of the SIRT2–S2iL5 and SIRT3–AceCS-KAc complexes.

(A) Structure of SIRT2 in complex with S2iL5. The SIRT2-specific insertion (residues 289–304) is colored magenta.

(B) Structure of SIRT3 in complex with AceCS-KAc (PDB ID 3GLR) (Jin et al., 2009).

The bound peptides are colored yellow, and the hydrogen bonds are shown as dashed green lines in (A) and (B).

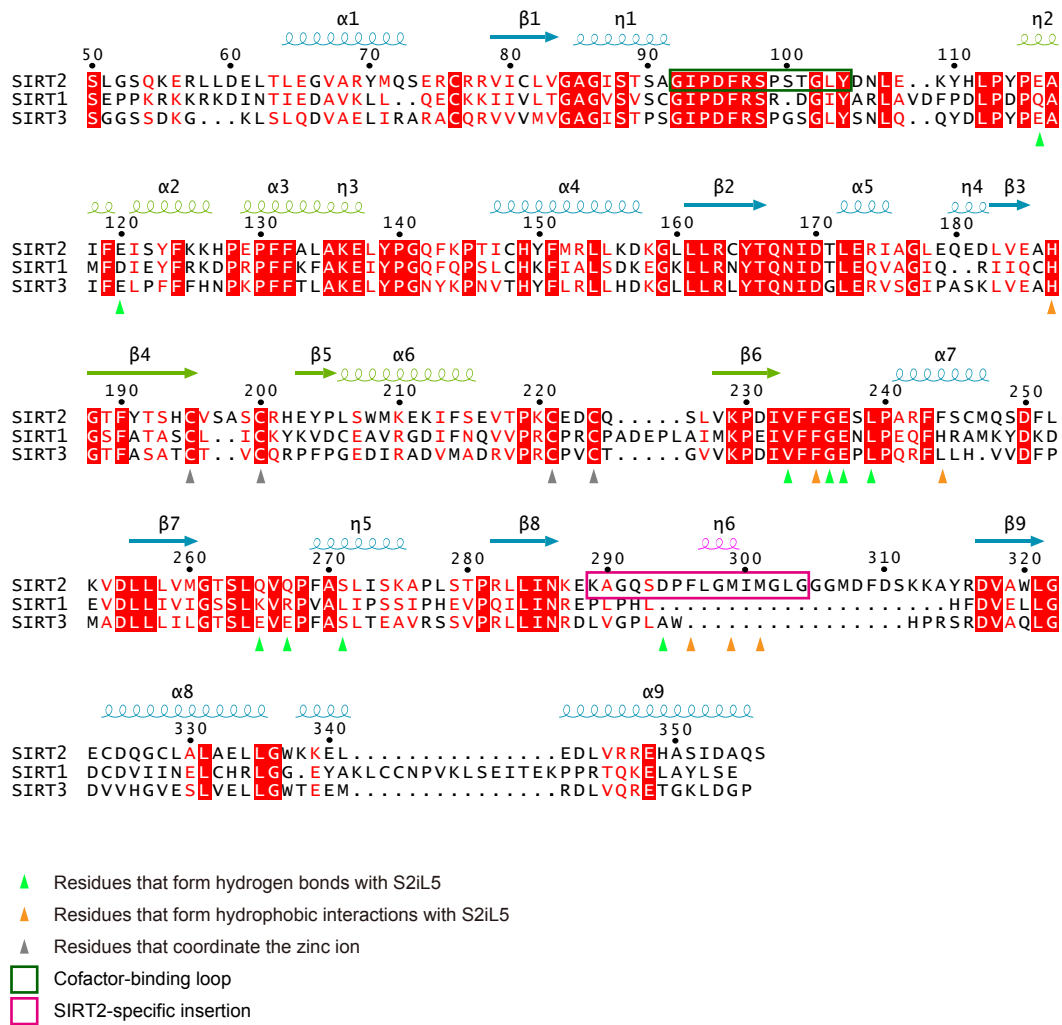


Figure 16 Sequence alignment of human SIRT1–SIRT3

The conserved residues are shown in red boxes. The secondary structure of SIRT2 is shown above the sequences. The cofactor-binding loop (residues 92–104) and the SIRT2-specific insertion (residues 289–304) are shown in green and magenta boxes, respectively. The figure was prepared using Toffee (Notredame et al., 2000) and ESPrIPT (Gouet et al., 1999).

Structural change upon S2iL5 binding

A comparison between the SIRT2 structures in complex with S2iL5 and in the free form ²⁶ revealed the conformational changes that occur in SIRT2 upon S2iL5 binding (Figure 17). First, the small domain moves toward the large domain upon S2iL5 binding, as observed in other sirtuins ²⁷⁻³² (Figure 17). This open-to-closed domain movement allows Phe235 to form the catalytic tunnel, and enables Gly236, Glu237 and Gln267 to form the β sheet-like interactions with S2iL5 (Figure 4B). Second, the SIRT2-specific insertion (residues 289–304) adopts a loop conformation to interact with S2iL5 in the S2iL5 complex, whereas it forms an α -helix in the free form ²⁶ (Figure 18). The side chain of Asp294 hydrogen bonds with the amide groups of Phe296 and Gly302, to stabilize the loop conformation. Third, S2iL5 binding induces a local conformational change, including the rotation of the side chains of Phe243 and Phe244, which are involved in the interactions with S2iL5 (Figure 18).

The crystal structure of SIRT2 in complex with ADP-ribose (ADPr), a product analog, was reported recently ³². A comparison between the SIRT2 structures in complex with S2iL5 and ADPr revealed that ADPr binding induces a local structural change in a so-called cofactor-binding loop (residues 92–104) (Figures 19 and 20A).

Residues 99–103 in the cofactor-binding loop are disordered in the S2iL5 complex, whereas they are ordered and involved in the recognition of ADPr in the ADPr complex. Phe96, Arg97 and Tyr104 interact with the nicotinamidic-ribose of ADPr, and Arg97 interacts with the phosphate group of ADPr. In addition, Lys287 in the large domain interacts with the adenine ring of ADPr. In SIRT3, the cofactor-binding loop adopts a closed conformation and Arg158 interacts with ADPr in the ADPr complex, whereas it adopts an open conformation in the free form and the AceCS-K^{Ac} complex (Jin et al., 2009) (Figure 20B). In contrast, in the SIRT2–S2iL5 complex, the cofactor-binding loop adopts a partially-closed conformation without cofactor binding, because Arg97 forms a salt bridge network with Glu116 in the small domain and R9 of S2iL5 (Figures 19 and 20A). Unlike the SIRT2–S2iL5 complex, Arg158 cannot form a salt bridge network with Glu177 and AceCS-K^{Ac} in the SIRT3–AceCS-K^{Ac} complex, since R9 of S2iL5 corresponds to M644 of AceCS-K^{Ac}.

The two domains in the ADPr complex adopt a closed conformation, as observed in the S2iL5 complex³² (Figure 17). However, in the ADPr complex, the SIRT2-specific insertion mimics a substrate peptide and interacts with the active-site groove of a neighboring SIRT2 molecule in the crystallographic asymmetric unit. This observation suggested that the closed conformation observed in the ADPr complex is

not due to ADPr binding, but rather to crystal packing interactions. This is consistent with the notion that the peptide substrate, but not the cofactor NAD⁺, induces an open-to-closed domain movement (Cosgrove et al., 2006). This mechanism was also reported for other sirtuins. The crystal structure of SIRT3, along with isothermal titration calorimetry experiments, indicated that the binding of the peptide substrate to SIRT3 supports the binding of NAD⁺ ²⁹. In addition, the crystal structures of a bacterial sirtuin revealed that the binding of the peptide substrate induces an open-to-closed domain movement ³³.

A comparison between the SIRT2 structures in the free form ²⁶ and in the complex with S2iL5 and ADPr ³² revealed that the SIRT2-specific insertion can adopt different conformations (Figure 17). A comparison between the S2iL5 and ADPr complexes indicated that the insertion loop in the ADPr complex interferes with the β sheet-like interaction between S2iL5 and SIRT2 in the S2iL5 complex (Figure 19), suggesting that the insertion loop in the ADPr complex is displaced for the substrate peptide binding. Given that this flexible SIRT2-specific insertion is involved in the interaction with S2iL5 (in the S2iL5 complex) and a neighboring SIRT2 molecule (in the free form and ADPr complex), it may play a role in the recognition of the substrate

peptides, although further studies will be required to elucidate its physiological function.

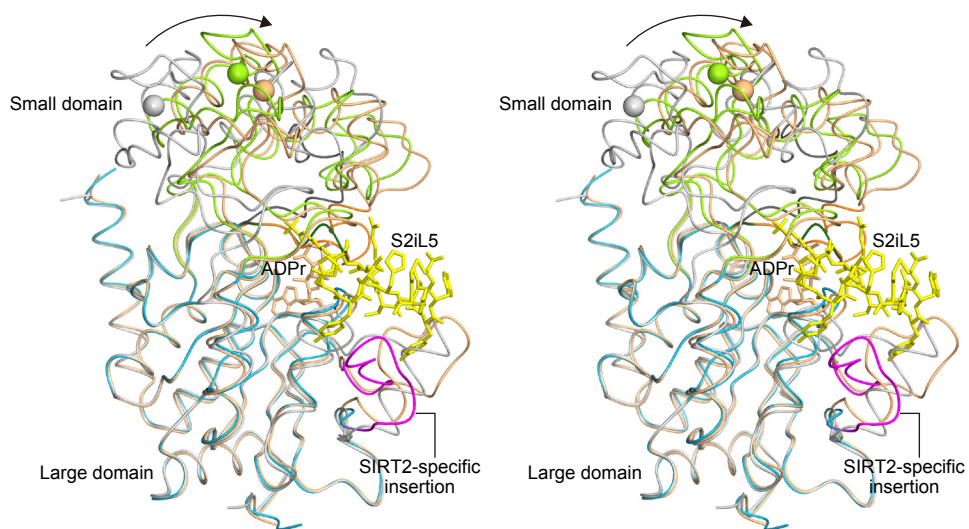


Figure 17 Structural change in SIRT2

Comparison between SIRT2 structures in the free form (PDB ID 1J8F; gray), and in complex with S2iL5 and ADPr (PDB ID 3ZGV; beige) (stereo view). The structures are superimposed based on their large domains. S2iL5 and ADPr are shown as stick models. The bound zinc ions are shown as spheres.

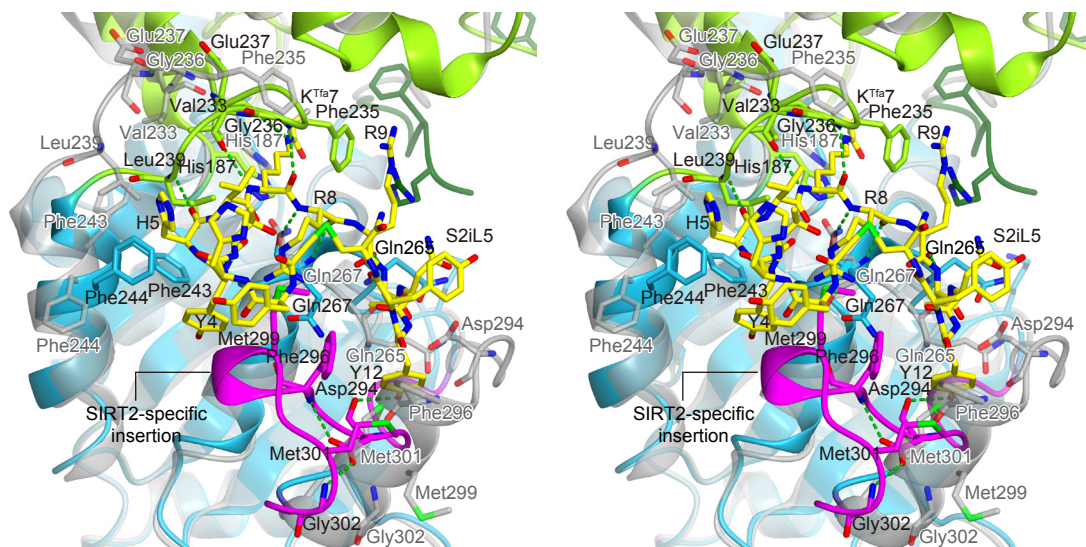


Figure 18 Close up of the structural change between SIRT2-S2iL5 complex and free form

Structural comparison of the S2iL5 complex with the free form (PDB ID 1J8F; gray) (stereo view).

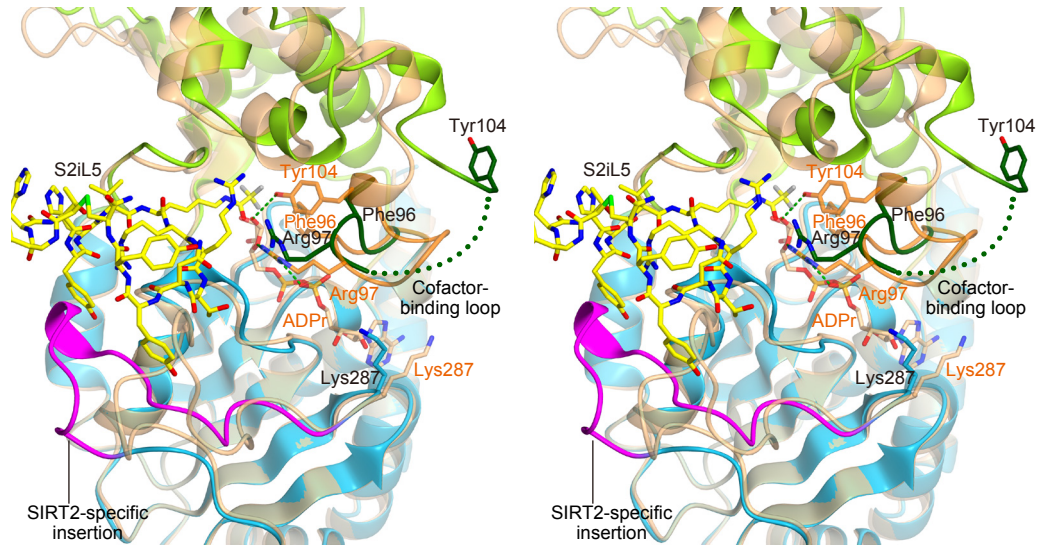


Figure 19 Close up of the structural change between SIRT2 in complex with S2iL5 and ADPr

Structural comparison of the S2iL5 complex with the ADPr complex (PDB ID 3ZGV; beige) (stereo view). The disordered region (residues 99-103) in the S2iL5 complex is indicated by green dots. SIRT2 and S2iL5 complex is colored as in Figure 7.

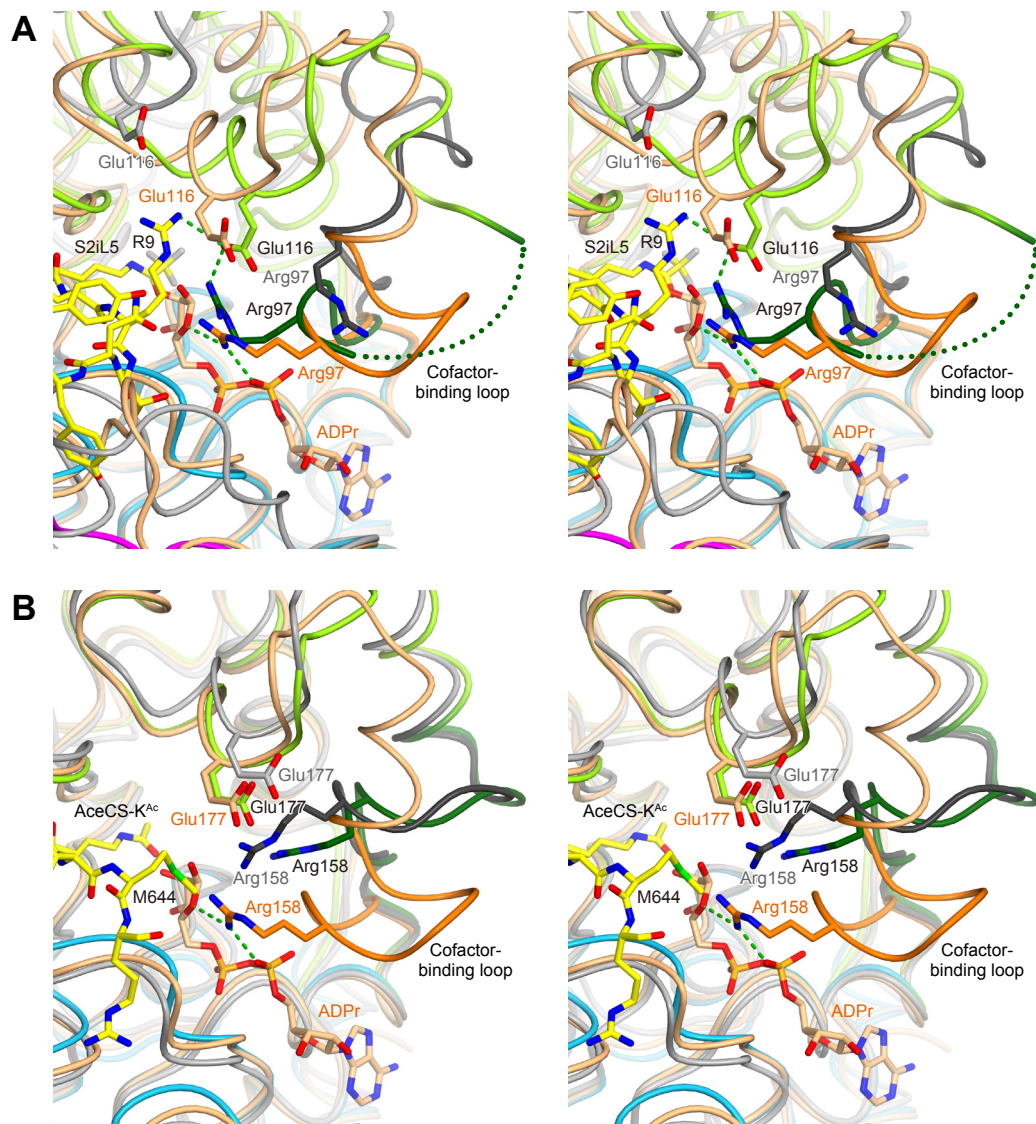


Figure 20 Structural comparison of the cofactor-binding loops in SIRT2 and SIRT3

(A) Superimposition of SIRT2 in the free form (PDB ID 1J8F; gray) and in the complex with S2iL5 (the same color code as in Figure 7) and ADPr (PDB ID 3ZGV; beige) (stereo view). The disordered region (residues 99–103) in the S2iL5 complex is indicated by green dots.

(B) Superimposition of SIRT3 in the free form (PDB ID 3GLS; gray) and in the complex with AceCS-KAc (PDB ID 3GLR; the same color code as in Figure 17B) and ADPr (PDB ID 4BN4; beige) (stereo view).

Mutational analysis

To confirm the functional significance of the observed interactions between SIRT2 and S2iL5, I determined the K_D values between S2iL5 and alanine mutants of SIRT2, by surface plasmon resonance (SPR) (Figures 11A and 12A). The F244A mutant showed the most pronounced reduction in the affinity for S2iL5 ($K_D = 4.0$ nM), confirming the importance of the interactions between Phe244 and S2iL5. The E116A and E120A mutants showed reduced affinity for S2iL5 ($K_D = 1.7$ and 2.2 nM, respectively), establishing the importance of the salt bridges between R9 of S2iL5 and Glu116 and Glu120 of SIRT2. The Q265A and S271A mutants showed reduced affinity for S2iL5 ($K_D = 1.8$ and 1.8 nM, respectively), confirming the importance of the hydrogen-bonding interactions between T10 and Gln265 and between Y4 and Ser271. The D294A mutant showed reduced affinity ($K_D = 1.4$ nM), suggesting the functional significance of the helix-to-coil transition in the SIRT2-specific insertion for S2iL5 binding. In contrast, the F296A, M299A and M301A mutants showed almost no reduction in their affinities for S2iL5, possibly because S2iL5 binds to SIRT2 through multiple interactions. I also determined the K_D values between SIRT2 and alanine mutants of S2iL5 (Figures 11B and 12B). Among the S2iL5 mutants tested, the R9A mutant showed the most pronounced reduction in the affinity for SIRT2 ($K_D = 7.9$ nM),

confirming the importance of the salt bridges between R9 of S2iL5 and Glu116 and Glu120 of SIRT2. This result is consistent with the increased K_D for the E116A and E120A mutants of SIRT2. The R8A mutant exhibited reduced affinity ($K_D = 3.8$ nM), verifying the functional significance of the PBI-like conformation of S2iL5, which is maintained by the R8-mediated intramolecular hydrogen-bonding network. The Y4A and H5A mutants showed reduced affinities ($K_D = 1.9$ and 2.4 nM, respectively). The Y4A/R9A/Y12A triple mutant showed an additive decrease in the affinity ($K_D = 29$ nM), as compared with the single mutants (Y4A, R9A and Y12A) and the double mutants (Y4A/R9A, R9A/Y12A and Y4A/Y12A). Notably, the Y4A/R9A/Y12A mutant showed markedly reduced affinity ($K_D = 29$ nM), as compared with the Y4A/R9A mutant ($K_D = 5.8$ nM), although the Y12A mutant showed no reduction in the affinity ($K_D = 0.42$ nM). These results indicated that the multiple interactions synergistically contribute to the binding of S2iL5 to SIRT2. I further determined the K_D values between SIRT2 and a 14-aa linear peptide, in which the amino group of Y1 in S2iL5 is acetylated, and a 5-aa short linear peptide corresponding to H5–R9 of S2iL5. The 14-aa linear peptide showed a marked decrease in the affinity ($K_D = 6.8$ nM), whereas the 5-aa linear peptide showed a drastic reduction in the affinity ($K_D = 145$ nM). Altogether, the mutational analyses

confirmed the functional significance of the observed binding mode between SIRT2 and S2iL5, and indicated the synergistic contributions of the multiple interactions.

Structural plasticity of macrocyclic peptide inhibitors

Using the RaPID system^{20,21}, I previously developed macrocyclic peptide inhibitors against a variety of enzymes, such as SIRT2 deacetylase¹⁹, E6AP ubiquitin ligase²⁰, and Akt2 kinase³⁴. These studies demonstrated the potential of the RaPID system for the discovery of macrocyclic peptide inhibitors with high selectivity and potency. However, their inhibitory mechanisms have remained unclear, since no crystal structure of an enzyme–macrocyclic peptide complex has been solved. Recently, the crystal structures of a MATE multidrug transporter in complex with *in vitro* selected macrocyclic peptides, MaD5 and MaL6, which selectively inhibit the drug extrusion activity of the MATE transporter has been reported³⁵. The structures revealed that MaD5 and MaL6 adopt lariat- and β -hairpin-like structures, respectively, to bind the central cleft of the transporter. Thus, the crystal structures of SIRT2 and MATE in complex with the macrocyclic peptides highlighted the structural plasticity of the macrocyclic peptides, which confers extremely high affinities to various target proteins.

Notably, the present structure of SIRT2 in complex with S2iL5 further revealed that S2iL5 binding induces an unanticipated conformational change in the flexible

SIRT2-specific region. The functional data demonstrated the potential role of this dynamic structural change for S2iL5 binding. It seems unlikely that small molecule inhibitors could induce such large structural changes in their target proteins, due to the limited number of inhibitor–protein interactions. Thus, the ability to bind to a target protein, by inducing a structural change within the target, is likely to be a unique advantage for macrocyclic peptide inhibitors³⁶.

I believe that the present structural information will be helpful for inventing drugs to improve ischemic conditions in the near future.

References

1. Sauve, A.A., Wolberger, C., Schramm, V.L. & Boeke, J.D. The biochemistry of sirtuins. *Annu Rev Biochem* **75**, 435-65 (2006).
2. Baur, J.A., Ungvari, Z., Minor, R.K., Le Couteur, D.G. & de Cabo, R. Are sirtuins viable targets for improving healthspan and lifespan? *Nat Rev Drug Discov* **11**, 443-61 (2012).
3. North, B.J. & Verdin, E. Sirtuins: Sir2-related NAD-dependent protein deacetylases. *Genome Biol* **5**, 224 (2004).
4. North, B.J., Marshall, B.L., Borra, M.T., Denu, J.M. & Verdin, E. The human Sir2 ortholog, SIRT2, is an NAD⁺-dependent tubulin deacetylase. *Mol Cell* **11**, 437-44 (2003).
5. Inoue, T., Hiratsuka, M., Osaki, M. & Oshimura, M. The molecular biology of mammalian SIRT proteins: SIRT2 in cell cycle regulation. *Cell Cycle* **6**, 1011-8 (2007).
6. Vaquero, A., Scher, M.B., Lee, D.H., Sutton, A., Cheng, H.L., Alt, F.W., Serrano, L., Sternglanz, R. & Reinberg, D. SirT2 is a histone deacetylase with preference for histone H4 Lys 16 during mitosis. *Genes Dev* **20**, 1256-61 (2006).
7. Narayan, N., Lee, I.H., Borenstein, R., Sun, J., Wong, R., Tong, G., Fergusson,

- M.M., Liu, J., Rovira, II, Cheng, H.L., Wang, G., Gucek, M., Lombard, D., Alt, F.W., Sack, M.N., Murphy, E., Cao, L. & Finkel, T. The NAD-dependent deacetylase SIRT2 is required for programmed necrosis. *Nature* **492**, 199-204 (2012).
8. Li, Y., Matsumori, H., Nakayama, Y., Osaki, M., Kojima, H., Kurimasa, A., Ito, H., Mori, S., Katoh, M., Oshimura, M. & Inoue, T. SIRT2 down-regulation in HeLa can induce p53 accumulation via p38 MAPK activation-dependent p300 decrease, eventually leading to apoptosis. *Genes Cells* **16**, 34-45 (2011).
9. Outeiro, T.F., Kontopoulos, E., Altmann, S.M., Kufareva, I., Strathearn, K.E., Amore, A.M., Volk, C.B., Maxwell, M.M., Rochet, J.C., McLean, P.J., Young, A.B., Abagyan, R., Feany, M.B., Hyman, B.T. & Kazantsev, A.G. Sirtuin 2 inhibitors rescue alpha-synuclein-mediated toxicity in models of Parkinson's disease. *Science* **317**, 516-9 (2007).
10. Chopra, V., Quinti, L., Kim, J., Vollor, L., Narayanan, K.L., Edgerly, C., Cipicchio, P.M., Lauver, M.A., Choi, S.H., Silverman, R.B., Ferrante, R.J., Hersch, S. & Kazantsev, A.G. The sirtuin 2 inhibitor AK-7 is neuroprotective in Huntington's disease mouse models. *Cell Rep* **2**, 1492-7 (2012).
11. Chen, L. Medicinal chemistry of sirtuin inhibitors. *Curr Med Chem* **18**, 1936-46

- (2011).
12. Disch, J.S., Evindar, G., Chiu, C.H., Blum, C.A., Dai, H., Jin, L., Schuman, E., Lind, K.E., Belyanskaya, S.L., Deng, J., Coppo, F., Aquilani, L., Graybill, T.L., Cuzzo, J.W., Lavu, S., Mao, C., Vlasuk, G.P. & Perni, R.B. Discovery of thieno[3,2-d]pyrimidine-6-carboxamides as potent inhibitors of SIRT1, SIRT2, and SIRT3. *J Med Chem* **56**, 3666-79 (2013).
 13. Napper, A.D., Hixon, J., McDonagh, T., Keavey, K., Pons, J.F., Barker, J., Yau, W.T., Amouzegh, P., Flegg, A., Hamelin, E., Thomas, R.J., Kates, M., Jones, S., Navia, M.A., Saunders, J.O., DiStefano, P.S. & Curtis, R. Discovery of indoles as potent and selective inhibitors of the deacetylase SIRT1. *J Med Chem* **48**, 8045-54 (2005).
 14. Nguyen, G.T., Schaefer, S., Gertz, M., Weyand, M. & Steegborn, C. Structures of human sirtuin 3 complexes with ADP-ribose and with carba-NAD⁺ and SRT1720: binding details and inhibition mechanism. *Acta Crystallogr D Biol Crystallogr* **69**, 1423-32 (2013).
 15. Gertz, M., Fischer, F., Nguyen, G.T., Lakshminarasimhan, M., Schutkowski, M., Weyand, M. & Steegborn, C. Ex-527 inhibits Sirtuins by exploiting their unique NAD⁺-dependent deacetylation mechanism. *Proc Natl Acad Sci U S A* **110**,

- E2772-81 (2013).
16. Schuetz, A., Min, J., Antoshenko, T., Wang, C.L., Allali-Hassani, A., Dong, A., Loppnau, P., Vedadi, M., Bochkarev, A., Sternglanz, R. & Plotnikov, A.N. Structural basis of inhibition of the human NAD⁺-dependent deacetylase SIRT5 by suramin. *Structure* **15**, 377-89 (2007).
 17. Zheng, W. Mechanism-based modulator discovery for sirtuin-catalyzed deacetylation reaction. *Mini Rev Med Chem* **13**, 132-54 (2013).
 18. Smith, B.C. & Denu, J.M. Acetyl-lysine analog peptides as mechanistic probes of protein deacetylases. *J Biol Chem* **282**, 37256-65 (2007).
 19. Morimoto, J., Hayashi, Y. & Suga, H. Discovery of macrocyclic peptides armed with a mechanism-based warhead: isoform-selective inhibition of human deacetylase SIRT2. *Angew Chem Int Ed Engl* **51**, 3423-7 (2012).
 20. Yamagishi, Y., Shoji, I., Miyagawa, S., Kawakami, T., Katoh, T., Goto, Y. & Suga, H. Natural product-like macrocyclic N-methyl-peptide inhibitors against a ubiquitin ligase uncovered from a ribosome-expressed de novo library. *Chem Biol* **18**, 1562-70 (2011).
 21. Hipolito, C.J. & Suga, H. Ribosomal production and in vitro selection of natural product-like peptidomimetics: the FIT and RaPID systems. *Curr Opin Chem*

- Biol* **16**, 196-203 (2012).
22. Huai, Q., Kim, H.Y., Liu, Y., Zhao, Y., Mondragon, A., Liu, J.O. & Ke, H. Crystal structure of calcineurin-cyclophilin-cyclosporin shows common but distinct recognition of immunophilin-drug complexes. *Proc Natl Acad Sci U S A* **99**, 12037-42 (2002).
23. Vagin, A. & Teplyakov, A. Molecular replacement with MOLREP. *Acta Crystallogr D Biol Crystallogr* **66**, 22-5 (2010).
24. Emsley, P. & Cowtan, K. Coot: model-building tools for molecular graphics. *Acta Crystallogr D Biol Crystallogr* **60**, 2126-32 (2004).
25. Adams, P.D., Grosse-Kunstleve, R.W., Hung, L.W., Ioerger, T.R., McCoy, A.J., Moriarty, N.W., Read, R.J., Sacchettini, J.C., Sauter, N.K. & Terwilliger, T.C. PHENIX: building new software for automated crystallographic structure determination. *Acta Crystallogr D Biol Crystallogr* **58**, 1948-54 (2002).
26. Finnin, M.S., Donigian, J.R. & Pavletich, N.P. Structure of the histone deacetylase SIRT2. *Nat Struct Biol* **8**, 621-5 (2001).
27. Avalos, J.L., Celic, I., Muhammad, S., Cosgrove, M.S., Boeke, J.D. & Wolberger, C. Structure of a Sir2 enzyme bound to an acetylated p53 peptide. *Mol Cell* **10**, 523-35 (2002).

28. Cosgrove, M.S., Bever, K., Avalos, J.L., Muhammad, S., Zhang, X. & Wolberger, C. The structural basis of sirtuin substrate affinity. *Biochemistry* **45**, 7511-21 (2006).
29. Jin, L., Wei, W., Jiang, Y., Peng, H., Cai, J., Mao, C., Dai, H., Choy, W., Bemis, J.E., Jirousek, M.R., Milne, J.C., Westphal, C.H. & Perni, R.B. Crystal structures of human SIRT3 displaying substrate-induced conformational changes. *J Biol Chem* **284**, 24394-405 (2009).
30. Du, J., Zhou, Y., Su, X., Yu, J.J., Khan, S., Jiang, H., Kim, J., Woo, J., Kim, J.H., Choi, B.H., He, B., Chen, W., Zhang, S., Cerione, R.A., Auwerx, J., Hao, Q. & Lin, H. Sirt5 is a NAD-dependent protein lysine demalonylase and desuccinylase. *Science* **334**, 806-9 (2011).
31. Zhou, Y., Zhang, H., He, B., Du, J., Lin, H., Cerione, R.A. & Hao, Q. The bicyclic intermediate structure provides insights into the desuccinylation mechanism of human sirtuin 5 (SIRT5). *J Biol Chem* **287**, 28307-14 (2012).
32. Moniot, S., Schutkowski, M. & Steegborn, C. Crystal structure analysis of human Sirt2 and its ADP-ribose complex. *J Struct Biol* **182**, 136-43 (2013).
33. Hoff, K.G., Avalos, J.L., Sens, K. & Wolberger, C. Insights into the sirtuin mechanism from ternary complexes containing NAD⁺ and acetylated peptide.

- Structure* **14**, 1231-40 (2006).
34. Hayashi, Y., Morimoto, J. & Suga, H. In vitro selection of anti-Akt2 thioether-macrocyclic peptides leading to isoform-selective inhibitors. *ACS Chem Biol* **7**, 607-13 (2012).
35. Tanaka, Y., Hipolito, C.J., D., M.A., Ito, K., Kuroda, T., Higuchi, T., T., K., Kato, E.H., Hattori, M., Kumazaki, K., Tsukazaki, T., Ishitani, R., Suga, H. & Nureki, O. Structural basis for the novel mechanism of drug extrusion by a MATE multidrug transporter. *Nature* **496**, 247-51 (2013).
36. Yamagata, K., Goto, Y., Nishimasu, H., Morimoto, J., Ishitani, R., Dohmae, N., Takeda, N., Nagai, R., Komuro, I., Suga, H. & Nureki, O. Structural Basis for Potent Inhibition of SIRT2 Deacetylase by a Macrocyclic Peptide Inducing Dynamic Structural Change. *Structure* (2013).

Acknowledgments

All of this study was performed at the Nureki laboratory (Department of Biophysics and Biochemistry, Graduate School of Science, The University of Tokyo) collaborating with the Suga laboratory (Department of Chemistry, Graduate School of Science, The University of Tokyo).

I would like to show my great thanks to Dr. Ryozo Nagai for providing me an opportunity to study at the Nureki laboratory. I also thank Dr. Issei Komuro for the advice for allowing to study at the Nureki laboratory.

At the Nureki laboratory, I would like to thank Dr. Osamu Nureki for allowing me to study at the laboratory, Dr. Ryuichiro Ishitani for the technical advice for the use of personal computers, and Dr. Hiroshi Nishimasu for teaching me the experimental technique.

At the Suga laboratory, I would like to thank Dr. Hiroaki Suga for letting us to collaborate with each other, Dr. Yuki Goto for the preparation of the peptides and the biochemical experiments.

I am grateful to the beam-line staff at BL32XU of SPring-8 for assistance in data collection. I also thank Dr. Ito and Dr. Yoshida for the gift of SIRT3 and Dr. Naoshi Dohmae for the MALDI-TOF MS experiment.

This work was supported by the Japan Society for the Promotion of Science (JSPS) through its “Funding Program for World-Leading Innovative R&D on Science and Technology (FIRST program)” to Dr. Osamu Nureki, by the Core Research for Evolutional Science and Technology (CREST) Program “The Creation of Basic Medical Technologies to Clarify and Control the Mechanisms Underlying Chronic Inflammation” of Japan Science and Technology Agency (JST) to Dr. Osamu Nureki, and by a grant for HPCI STRATEGIC PROGRAM Computational Life Science and Application in Drug Discovery and Medical Development by MEXT to Dr. Ryuichiro Ishitani. This work was also supported by a JSPS Grant-in-Aid for Specially Promoted Research (21000005) to Dr. Hiroaki Suga.